Final for AOARD Grant 114041

"Surface De-wetting Based Critical Heat Flux Model Development and Validation"

Date: February, 5, 2013

Name of Principal Investigators (PI): Sung Jin Kim
- e-mail address : sungjinkim@kaist.ac.kr
- Institution : KAIST
- Mailing Address : KAIST, Mechanical Engineering Building 5111, 373-1 Guseong-dong, Daejeon 305-701, Republic of Korea
- Phone : 82-42-350-3043
- Fax : 82-42-350-8207

Name of Principal Investigators (Co-PIs): Jungho Kim
- e-mail address : kimjh@umd.edu
- Institution : University of Maryland
- Mailing Address : University of Mary land, Department of Mechanical Engineering Building 88, College Park, MD, 20742 USA
- Phone : 1-301-405-5437

Period of Performance: 05/01/2011 ~ 07/31/2012

Report Documentation Page

Form Approved
OMB No. 0704-0188

1. REPORT DATE	2. REPORT TYPE	3. DATES COVERED
15 FEB 2013	**Final**	**06-06-2011 to 05-02-2013**

4. TITLE AND SUBTITLE
Surface De-Wetting Based Critical Heat Flux Model Development

5a. CONTRACT NUMBER
5b. GRANT NUMBER
5c. PROGRAM ELEMENT NUMBER

6. AUTHOR(S)
Sung Jin Kim

5d. PROJECT NUMBER
5e. TASK NUMBER
5f. WORK UNIT NUMBER

7. PERFORMING ORGANIZATION NAME(S) AND ADDRESS(ES)
Korea Advanced Institute of Science and Technology,373-1, Guseong-dong,,Yuseong-gu, Daejeon 305-701,Korea,NA,NA

8. PERFORMING ORGANIZATION REPORT NUMBER
N/A

9. SPONSORING/MONITORING AGENCY NAME(S) AND ADDRESS(ES)
AOARD, UNIT 45002, APO, AP, 96338-5002

10. SPONSOR/MONITOR'S ACRONYM(S)
AOARD

11. SPONSOR/MONITOR'S REPORT NUMBER(S)
AOARD-114041

12. DISTRIBUTION/AVAILABILITY STATEMENT
Approved for public release; distribution unlimited

13. SUPPLEMENTARY NOTES

14. ABSTRACT
Experimental work was undertaken to investigate the critical heat flux (CHF) mechanism in pool boiling. Local temperature and heat transfer coefficient on the heated surface were measured via IR camera. Based on the experimental results, the wetted area fraction and the contact line length density with wall superheat were observed. Also, an analytical work into pool boiling heat transfer was presented to determine the contribution of each region to the overall heat transfer in pool boiling. The heat transfer through the liquid was found to be the dominant heat transfer mechanism due to significantly larger area. While the heat transfer through the liquid determines the overall heat transfer, contact line heat transfer wall is critically important to trigger the onset of CHF. When the process of dewetting occurs at contact line and micro region, the temperature of dry spots increases, hence dryout areas increase and the CHF occurs. Finally, we proposed the CHF mechanism based on the surface dewetting and experimental data.

15. SUBJECT TERMS
spray cooling, spray cooling, Modelling & Simulation, thermal transport , Thermophysics

16. SECURITY CLASSIFICATION OF:			17. LIMITATION OF ABSTRACT	18. NUMBER OF PAGES	19a. NAME OF RESPONSIBLE PERSON
a. REPORT	b. ABSTRACT	c. THIS PAGE			
unclassified	**unclassified**	**unclassified**	**Same as Report (SAR)**	**16**	

ABSTRACT

Experimental work was undertaken to investigate the critical heat flux (CHF) mechanism in pool boiling. Local temperature and heat transfer coefficient on the heated surface were measured via IR camera. Based on the experimental results, the wetted area fraction and the contact line length density with wall superheat were observed. Also, an analytical work into pool boiling heat transfer was presented to determine the contribution of each region to the overall heat transfer in pool boiling. The heat transfer through the liquid was found to be the dominant heat transfer mechanism due to significantly larger area. While the heat transfer through the liquid determines the overall heat transfer, contact line heat transfer wall is critically important to trigger the onset of CHF. When the process of dewetting occurs at contact line and micro region, the temperature of dry spots increases, hence dryout area increases and the CHF occurs. Finally, we proposed the CHF mechanism based on the surface dewetting and experimental data.

INTRODUCTION

Critical heat flux (CHF) is the maximum heat flux at which nucleate boiling heat transfer sustains high cooling efficiency. Above the CHF value, the surface becomes covered with a vapor film that prevents the ambient liquid from contacting the wall, resulting in an increase in the wall temperature and subsequent system failure if the temperature exceeds the limits of the materials in the system. For this reason, systems incorporate a safety margin by operating at a heat flux much lower than the CHF, even though this reduces their efficiency. This compromise between safety and efficiency is an important issue in thermal systems such as cooling of electronics, nuclear power plants, and x-ray sources. Techniques to increase the heat transfer from surfaces must be based on proper understanding of the mechanisms involved so the proper mechanisms can be exploited. Although numerous models for critical heat flux have been presented over the years (e.g., bubble crowding, hot-spot formation, hydrodynamic instability mechanisms, and liquid macrolayer dryout), none can be used to explain the majority of the data.

The objectives of this work are to clarify the CHF mechanism in pool boiling through experiments and corresponding analysis. Reviews of the mechanisms and available data are briefly covered, then a new CHF mechanism based on surface de-wetting is described. This mechanism is based on new experimental data that has been acquired using an infrared (IR) camera to measure the local temperature and heat flux on superheated walls. A brief review of some of the proposed models along with their shortcomings is given below.

Bubble crowding model. This model suggests the number of individual bubbles on the surface increases with wall superheat and limits the supply of liquid to the wall. The bubbles are assumed to be spherical and pack the wall. The problem with this model is that the small, individual bubbles observed in the nucleate boiling regime are observed to merge vertically and laterally during boiling forming columns and large coalesced bubbles as the heat flux is increased, and do not cover the surface with a layer of small bubbles.

Helmholtz instability model. In the model proposed by Kutateladze [1948] and refined by Zuber [1959], the surface is assumed to be covered by an array of escaping vapor jets whose spacing is given by the wavelength that amplifies most rapidly ($\lambda_D = \sqrt{3}\lambda_C$ where λ_C is the critical wavelength, Figure 1). The

vapor/liquid interface can become Helmholtz unstable if the velocity difference between the vapor and the surrounding liquid exceeds a certain value, causing vapor to blanket the surface and drastically reducing the heat transfer. This model has been quite popular as it gives reasonable predictions for large, upward facing heaters. It is a purely hydrodynamic model, however, that makes certain specific assumptions regarding the geometry of the vapor columns and their spacing. It also does not contain any information about the affinity of the liquid for the surface, and cannot predict the effects of changing contact angle on CHF. This is in direct contradiction with much of the data in the literature that show an increase in CHF with an increase in surface wetting (decrease in the contact angle).

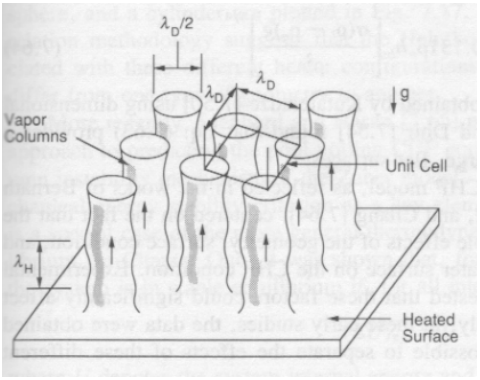

Figure 1: Schematic illustrating the hydrodynamic instability model parameters

Macrolayer model. Haramura and Katto's [1983] model focuses on the behavior of the thin liquid layer (the macrolayer) trapped between the wall and a large, coalesced bubble that forms from the merger of vapor generated at numerous nucleation sites (Figure 2). The thickness of the liquid was assumed to be λ_H /4 (λ_H is the Helmholtz wavelength), and the large coalesced bubbles were spaced λ_D apart. The model assumes that CHF occurs if the hovering time of the coalesced bubble is longer than the time it takes for the macrolayer to evaporate. The form of the equation they derived was similar to that of Zuber's if the ratio of the area of the vapor to wetted area was . Like the Zuber model, this model also does not contain any information regarding the fluid/wall interactions, and has also been questioned since some researchers have found that the liquid layer could be continually replenished through a network of liquid channels underneath the coalesced bubble.

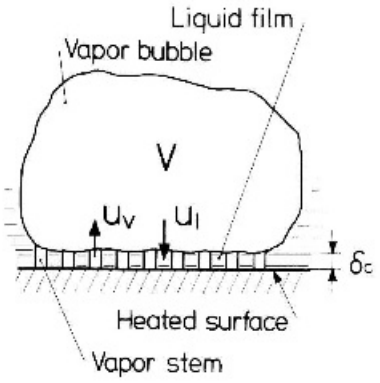

Figure 2: Macrolayer model schematic

Kandlikar model. More recent research has focused on the effect of surface wetting on CHF, and attempts to explain the decrease in CHF with increasing contact angle. In the extreme, CHF decreases to zero on non-wetting surfaces, a trend that cannot be predicted using the Zuber or Haramura and Katto models. These models also cannot explain the effect a coating of nanoparticles has on increasing CHF. Kandlikar [2001] developed a model that assumes CHF occurs when the unbalanced forces acting at the three-phase contact line of a bubble (surface tension, momentum of the incoming liquid, vapor recoil force due to evaporation, and the hydrostatic pressure) result in spreading of the vapor on the surface. He was able to derive a CHF relation that includes the effect of contact angle and orientation of the surface relative to the gravity vector. One problem with this model is that the apparent contact angle at the three-phase contact line changes with wall temperature, as will be discussed below. There are also doubts about the importance of the vapor recoil force that appears to play a pivotal role in this model.

Contact line models. Nishio and Tanaka (2004) used a total internal reflection (TIR) technique to directly observe the liquid distribution during boiling of R-113 on a 5 mm thick, single-crystal sapphire surface. The bottom of the sapphire was heated by supplying a DC current through a conductive transparent coating. The angle between the xenon light source and the sapphire was such that total internal reflection of light occurred if the top of the sapphire were dry and no reflection occurred if the surface was wet. This allowed clear images to be obtained of the wet and dry regions. Data were obtained from nucleate boiling through CHF and into film boiling. Through image processing, they were able to measure the wetted area fraction along with the length of the three-phase contact line. The wetted area fraction decreased monotonically with wall superheat and no correlation with wall heat flux was observed. The contact line length, however, increased as the wall superheat increased, peaked at CHF, then decreased for temperatures above T_{CHF} (Figure 3), indicating a direct correlation between the two.

CHF for spray cooling. The behavior of the thin film formed during spray cooling could be thought of as analogous to the macrolayer under the hovering, coalesced bubble, but with much more disturbance from the incoming liquid droplets. Horacek et al. [2005] observed a flow structure similar to that observed by Nishio and Tanaka [2004] when using the TIR technique to image the liquid-vapor on the wall in spray cooling. A microheater array built on a transparent silica substrate allowed for visualization of the impacting spray in conjunction with local heat transfer measurements. They found that the average fraction of the heater surface wet by liquid was a function of wall superheat, and indicated that the wetted area fraction monotonically decreased as the wall superheat increased. The amount of liquid on the surface correlated with wall superheat and not with heat flux. If CHF were taken to occur at an average superheat of 30°C, the corresponding wetted area fraction was about 0.45. This is close to the wetted area fraction of 0.40 at CHF obtained in Nishio and Tanaka's pool boiling study. There was a strong correlation between the contact line length and the heat flux, however. CHF occurs at the highest contact line length density. It is unknown at this time whether heat is transferred at the contact line by the thin film heat transfer mechanisms suggested by Wayner et al. [1976] or by an alternate mechanism such as transient conduction into the liquid as it moves over the surface as has been proposed for pool boiling Demiray and Kim, [2004].

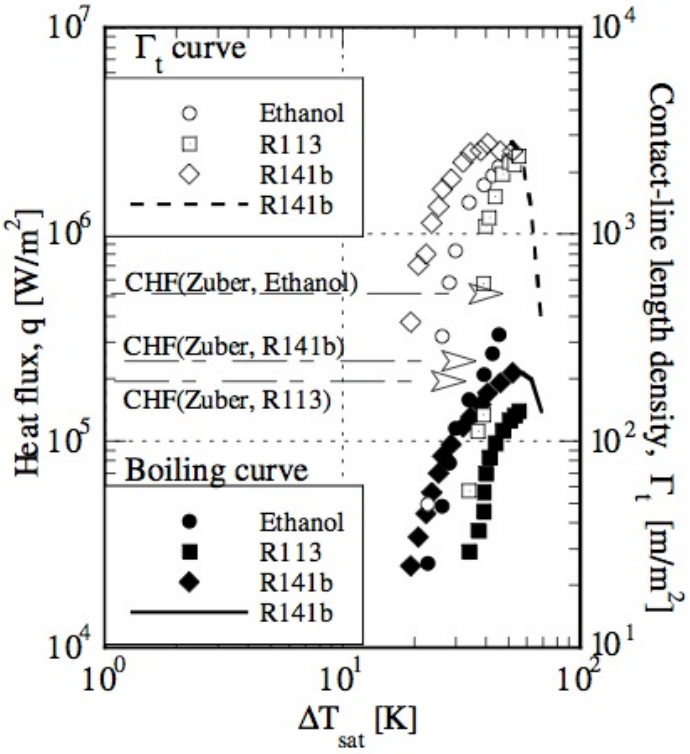

Figure 3: Heat flux and contact line length density variation, from Nishio and Tanaka (2004)

Further experiments which directly manipulate the contact line length in both a static and dynamic configuration are needed to elucidate which of these mechanisms might be responsible.

Spray cooling heat transfer should not be limited by any of the above mechanisms since removal of vapor generated from the surface is not a problem. No hydrodynamic instability exists in spray cooling, nor does a coalesced bubble hover over the surface to limit the supply of liquid to the macrolayer. According to these two models, CHF in spray cooling should be limited simply by the supply of liquid to the wall. Heat fluxes calculated from such an energy balance, however, result in much higher values than are typically observed. The heat flux is highest directly under the spray and decreases with increasing radial distance. It is interesting to note that the temperature at which CHF occurs remains relatively constant (about 90°C for this particular fluid/surface combination) despite the large variation in liquid flow rate to the surface.

Effect of wall superheat on contact angle. One last area to be reviewed that has been relatively neglected in boiling research, but which is important for understanding the proposed CHF mechanism, is the effect of wall superheat on the contact angle. Fluids such as FC-72 on copper typically have contact angles that are very small, perhaps 10° if the temperature of the substrate is lower than the saturation temperature. It has been observed by numerous researchers, however, that the contact angle can increase significantly if the wall is heated to above the saturation temperature. An example of this along with a thermodynamic justification was provided by Elbaum et al. [1995]. To confirm this, we measured the apparent contact angle of evaporating FC-72 droplets onto copper surfaces oxidized to varying degrees (Figure 4). As the wall superheat increases from 0°C to about 15°C (the maximum

superheat we could go to without nucleation occurring in the droplets), the contact angle is observed to increase from about 9° to over 40° in some cases. Although this behavior has significant implications for modeling of nucleate boiling and CHF, it has been completely neglected to date. These results have been published in Raj et al. [2012].

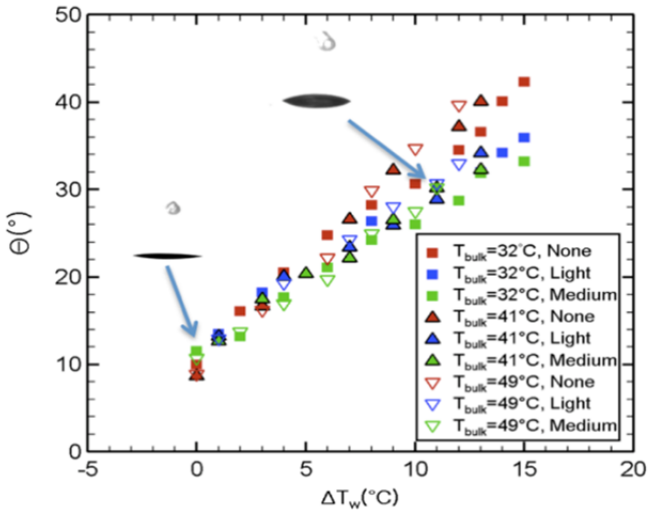

Figure 4: Contact angle vs. superheat at three bulk liquid temperatures and three oxidation levels on copper surface under saturated vapor environment.

EXPERIMENT

A description of the experimental apparatus and measurement techniques are described below. The techniques rely on a technique developed by Kim at al.[2011] to obtain local temperature and heat flux data using an IR technique.

Apparatus. A schematic diagram of the pool-boiling experimental facility is shown in Fig. 5. It consists of an actual boiling pool, and a heating section. The test fluid is FC-72, a highly-wetting dielectric perfluorocarbon. The main test chamber is a stainless steel pressure vessel, 250 mm high and 180 mm diameter. Cartridge heaters are immersed in the liquid to control the working fluid temperature. Atmospheric pressure is maintained by venting the vessel to ambient. Polycarbonate windows, 10-mm thick and with a maximum allowable temperature of 140°C, are placed in the front and back walls of the pool to visualize the boiling phenomenon on the test heater. A reflux condenser is located at the top of the pool to condense the phase-changed vapor back into liquid. Type-K thermocouples are placed within the test chamber to measure the working fluid temperature. During the experiment and degassing, the bulk temperature is maintained at saturation condition using feedback control based on the thermocouples and the cartridge heaters. The test sample is located at the bottom of the pool. An IR camera views the bottom of the test sample and measures the energy emitted by the test heater. For the boiling experiments, the test sample is heated by a computer controlled DC power supply connected. All test data were measured with a computer controlled data acquisition system.

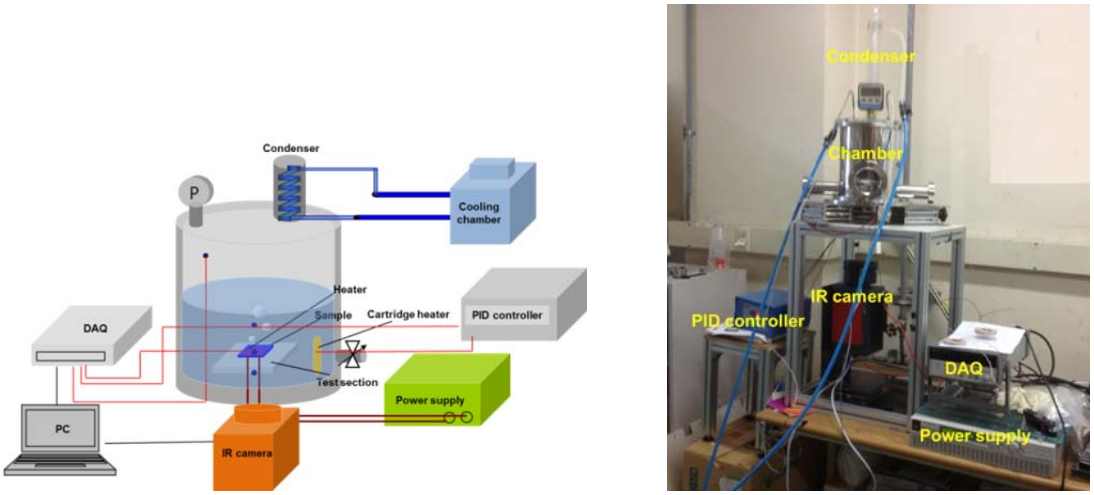

Figure 5: Pool boiling experimental facility

Test heater. The test heater design, shown in Fig. 6, was a multilayer wall consisting of a silicon substrate (44 mm $\times$ 20 mm $\times$ 1 mm) onto which polyimide tape (34 μm thickness) with acrylic adhesive was attached. The polyimide tape was necessary to measure heat transfer coefficient distributions of the expected magnitude. An opaque black paint much thinner (6 μm thickness) than the other layers was applied to the top of the polyimide tape. The high carbon black content ensured the coating is opaque, and its high thermal conductivity relative to the polyimide and thinness allowed its temperature to be assumed to be uniform. The black surface was exposed to the liquid pool. The heater assembly was attached to a polyether ether ketone (PEEK) baseplate using a 3M epoxy to insulate the sidewall. The resistor of silicon was measured using a four-point-probe. The measured voltage across the test heater and the current determined from the measured voltage across a resistor was used to calculate the heat flux applied to the test heater.

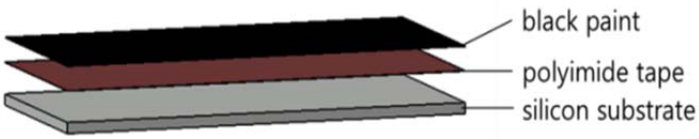

Figure 6: Test heater design

Measurement techniques. A midwave IR camera (3.6 μm - 5.1μm) was used to measure the temperature variations within the multilayer using a technique developed by Kim at al. [2011]. Since the energy measured by the IR camera consisted of emission from the black surface, emission from each of the layers and reflection from the surroundings, the total energy measured by the camera was sum of the energies emitted by each layer within the spectral bandwidth of the IR camera. To obtain the temperature and heat transfer coefficient at the fluid-wall interface, the temperature gradient was needed. The temperature profiles within the multilayer were not known initially, but could be obtained by solving the coupled conduction and radiation equations.

Test procedure. Prior to all testing, the test chamber was heated to the test liquid's saturation temperature using the cartridge heater. Once at saturation, the test liquid was boiled vigorously for at least two hours to remove dissolved gases. After

degassing, the external condenser was turned off. With the system still open to ambient, some of the test liquid was allowed to escape in order to push out any trapped air at the top of the condenser. The measured temperature and pressure readings within the test chamber were checked against the FC-72 saturation curve to ensure that all non-condensable was removed. The desired system pressure was then established by controlling the bulk fluid temperature using the internal condenser. After the desired pressure was obtained testing began. All of the test surfaces were tested in the horizontal, upward facing orientation.

The data acquisition consisted of two custom computers. One computer was equipped with Labview software to control the heat flux in the experimental rig and collect data. The second computer recorded the data from an Electrophysics Silver 660M mid-range infrared camera.

RESULTS AND DISCUSSION

Local temperature and heat flux. All data were obtained with the saturation temperature for FC-72 at T_{bulk} = 56 ^{o}C for ambient pressures (P = 1 atm). The local heat flux from surface and temperature in pooling boiling were deduced from the IR data. The heat transfer and temperature variations at a typical point on the surface near critical heat flux (15.9 W/cm^2) are shown on Figure 7. The temperature and heat flux fluctuate as bubbles are generated, the surface dries out, and liquid rewets the surface. Starting around t=5.7 s, though, the temperature increases and the heat transfer decreases to near zero as dryout occurs and the surface transitions through CHF. Advancing liquid during the liquid rewetting process results in much higher heat transfer than when liquid has covered the surface for some time or when the surface is drying out since the dryout area suddenly is cooled by the advancing liquid, much like during quenching.

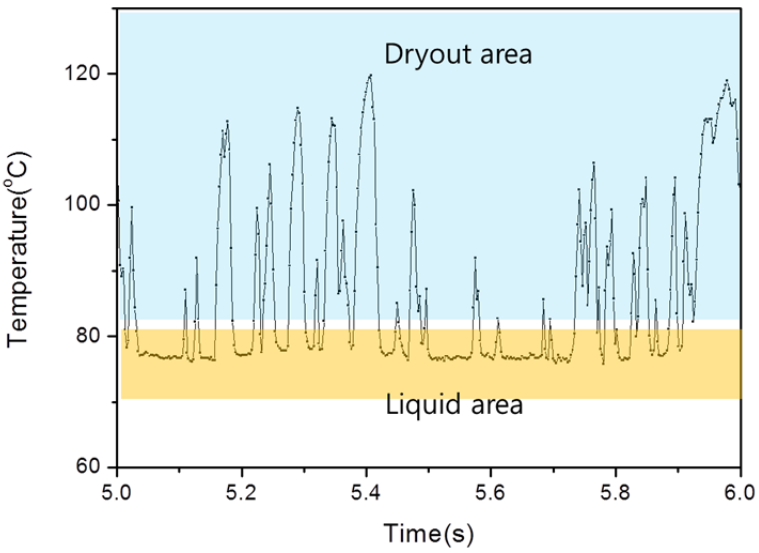

(a) Local temperature

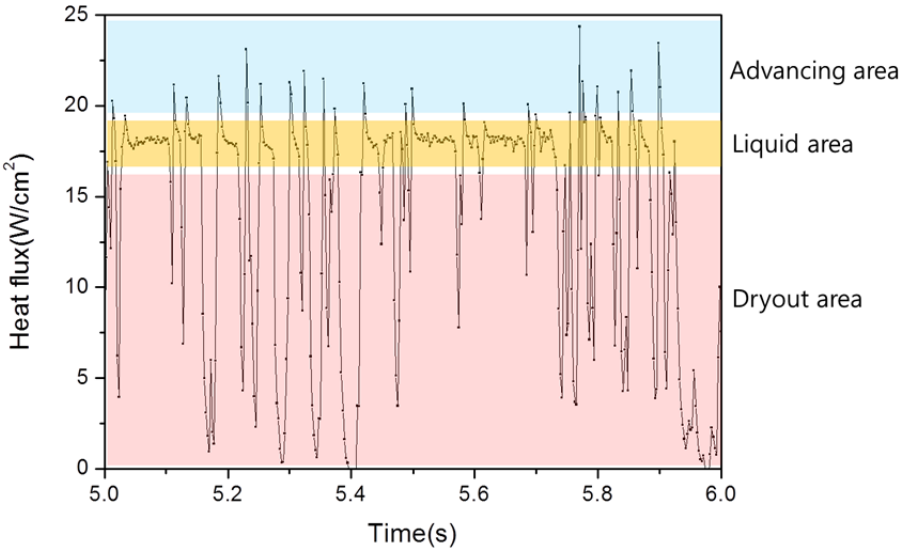

(b) Local heat flux

Figure 7: Local temperature and flux from a typical point on the surface at q"=15.9 W/cm^2 (P = 1 atm)

Time resolved temperature and heat flux distributions on the wall during pool boiling were obtained as shown in Fig. 8 (single frame), and illustrates the high spatial and temporal resolution that can be attained using the IR technique. The development of regions of low heat transfer and high temperature indicating dry spots are observed. As vapor departs the surface, and the dry spots shrink and higher heat transfer is observed the departure areas as they are rewet by the bulk liquid. Just prior to critical heat flux, it is observed that local dry spots appear at various locations on the heating surface and then disappear due to rewetting. When the rewetting process is somehow hindered, local dry spots grow and CHF occurs.

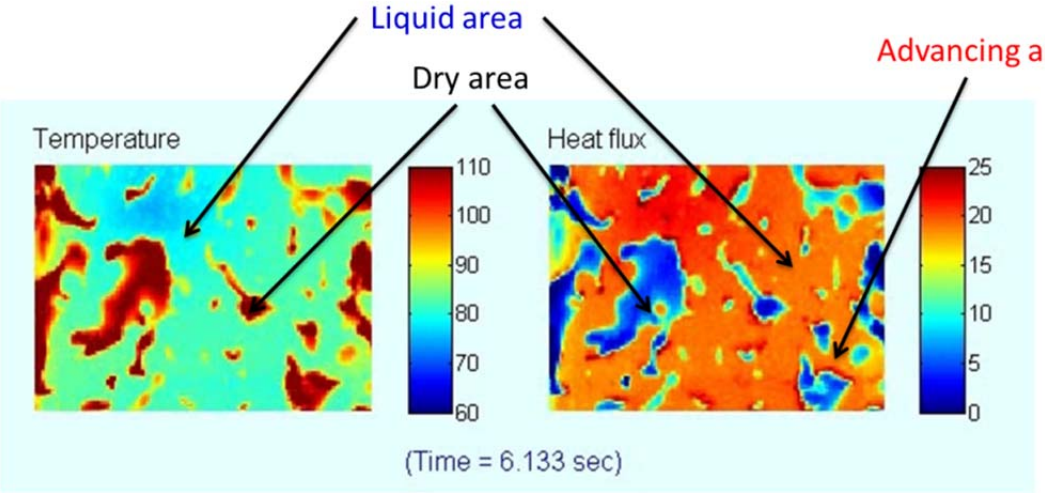

Figure 8: Temperature and heat flux distribution at q"=15.9W/cm^2

The area averaged values for temperature and heat flux were computed. The temperature increases and the heat flux decreases at CHF value (Figure 9(a)) as would be expected. The average surface temperature increases since the dryout area temperature increases as the average lifetime of a dry spot is increased by dewetting

process at CHF as shown in Fig. 9(b). The heat flux from the surface had a negative linear relation with the surface temperature using Pearson's product moment coefficient, meaning the surface temperature decreases as the heat transfer from the surface increases.

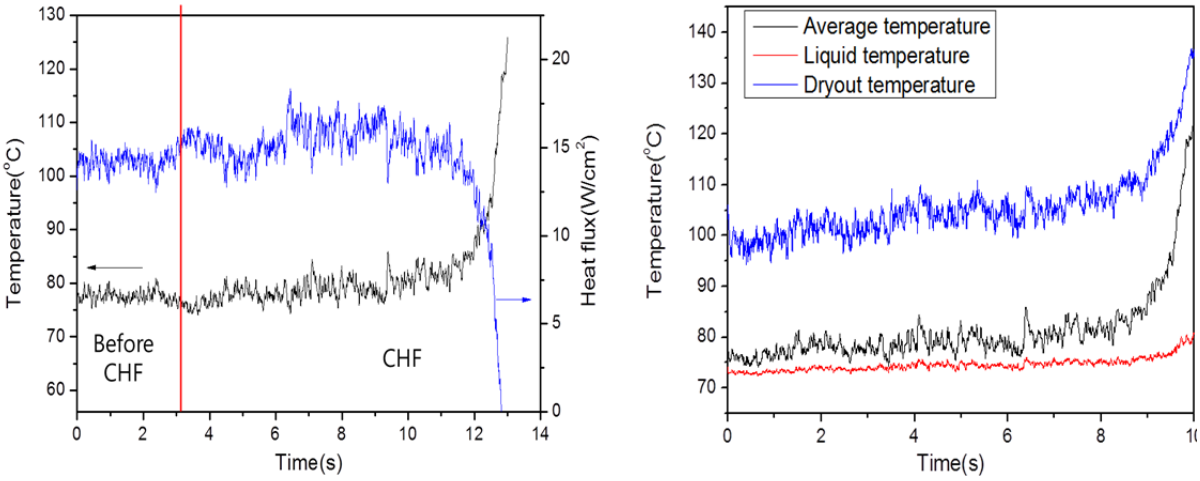

(a) Area averaged heat flux and temperature (b) Averaged temperature for each area

Figure 9: Area averaged temperature and heat flux behavior with time scale at q"=15.9W/cm^2

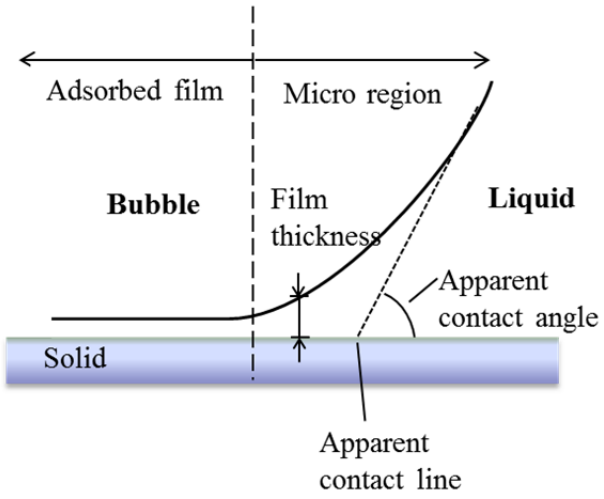

Figure 10: Sketch of the micro region at the contact line**.**

Apparent contact line and wetted area fraction. The microscopic region at the contact line where the liquid-vapor interface meets the solid wall is critically important to the heat and mass transfer during evaporation. A sketch of the microscopic region at the contact line is shown in Fig. 10. The micro region is defined as the region in which the adhesion forces between fluid molecules and wall molecules, and the effect of the curvature of the vapor–liquid interface on the local thermodynamic equilibrium are important. Ahead of micro region, there is an adsorbed layer of molecules on the solid wall known as the adsorbed film. No evaporation takes place in this region due to the strong attractive forces between the fluid and the wall. In the micro region, the curvature suddenly increases, the thickness of the liquid film starts to grow, and heat and mass transfer occurs

vigorously. The vapor pressure at the liquid–vapor interface can strongly deviate from the pressure in the macroscopic domain due to the high values of curvature, and the disjoining pressure accounts for attraction forces and the recoil pressure. Liquid flows into micro region from the macroscopic domain due to the large pressure jump in the micro region that forms as a result of evaporation losses.

The length scale of the micro region is very small and only the apparent contact line can be observed experimentally. The wetted area fraction and the location of the contact line can be obtained from the heat flux distribution as follows:

$$dq''_o = \sqrt{\left(\frac{q''_{o-dx} - q''_{o+dx}}{2\,dx}\right)^2 + \left(\frac{q''_{o-dy} - q''_{o+dy}}{2\,dy}\right)^2} \quad (1)$$

where q" is heat flux, and *dx* and *dy* are the pixel size. At the contact line, the values of Eq. (1) have different order with liquid and vapor region since the change of heat flux is much larger. Once the apparent contact line location was found, the wetted area and the dryout area were determined. Here, the definition of the wetted area fraction is the ratio of the wetted area to total area and the contact line length density is the contact line length divided by total area. The wetted area fraction and the contact line length density variation with wall superheat are shown in Fig. 11. With increases in wall superheat, the rate of heat transfer into the vapor bubble increases, so the bubble growth and the wetted area fraction decrease monotonically with wall superheat. The contact line length, however, increases with wall superheat and is maximum at CHF. The wetted area fraction has a negative linear relation with the surface temperature, i.e., the wetted area fraction decreases as the heat transfer from the surface decreases or the surface temperature increases.

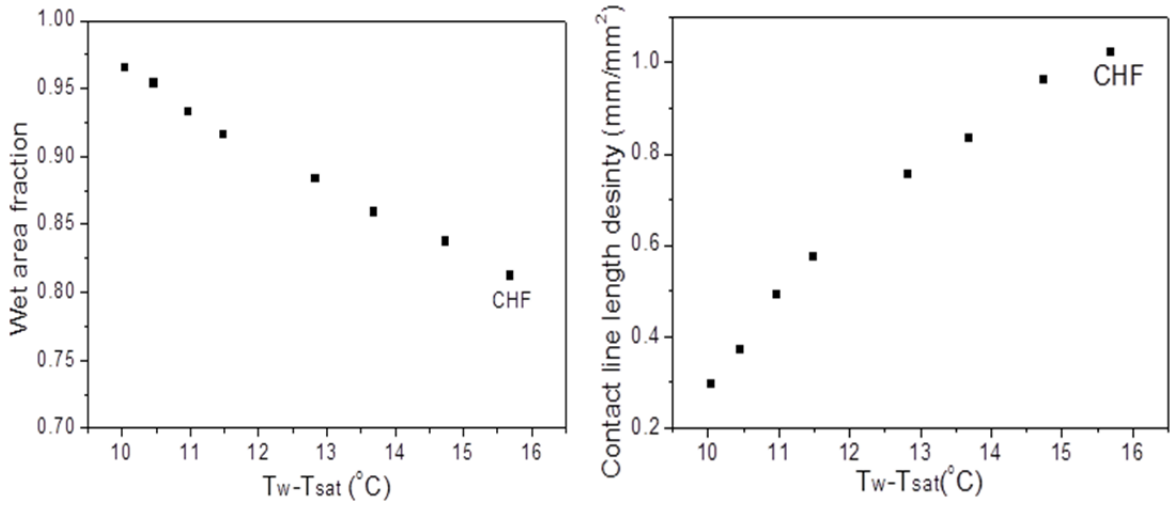

(a) Wet area fraction (b) Contact line length density

Figure 11: Wet area fraction and contact line length density change with wall superheat at T_{bulk} = 56 °C for ambient pressures.

Heat transfer regions. Numerous mechanisms are available through which energy is transferred from the wall in pool boiling. Evaporation of the liquid at the contact line contributes to dryout growth (receding regime). Transient conduction

into the advancing liquid front occurs as the dry patch is rewet (advancing regime). Energy is transferred by convection and conduction where vapor and liquid cover the surface (dryout regime, liquid regime). Based on the heat flux and temperature data, the heat transfer from each region such as dryout area, liquid area, advancing area, and receding area (the various regimes are shown in Figure 12) were measured in pool boiling. This data indicated that heat flux that occurs as liquid rewets the surface results in the highest heat flux. However, the largest contributor to the overall boiling heat transfer is heat transfer through the liquid regime which accounts for over 90% of the total heat transfer since it has the largest area associated with it (Figure 13). The averaged advancing area and receding area with wall superheat were measured. It is observed that with the increase in wall superheat, the evaporation of liquid becomes more intense (receding area increases), and more fluid must be delivered to the contact line to feed this evaporation (advancing area increases) as shown in Fig. 14.

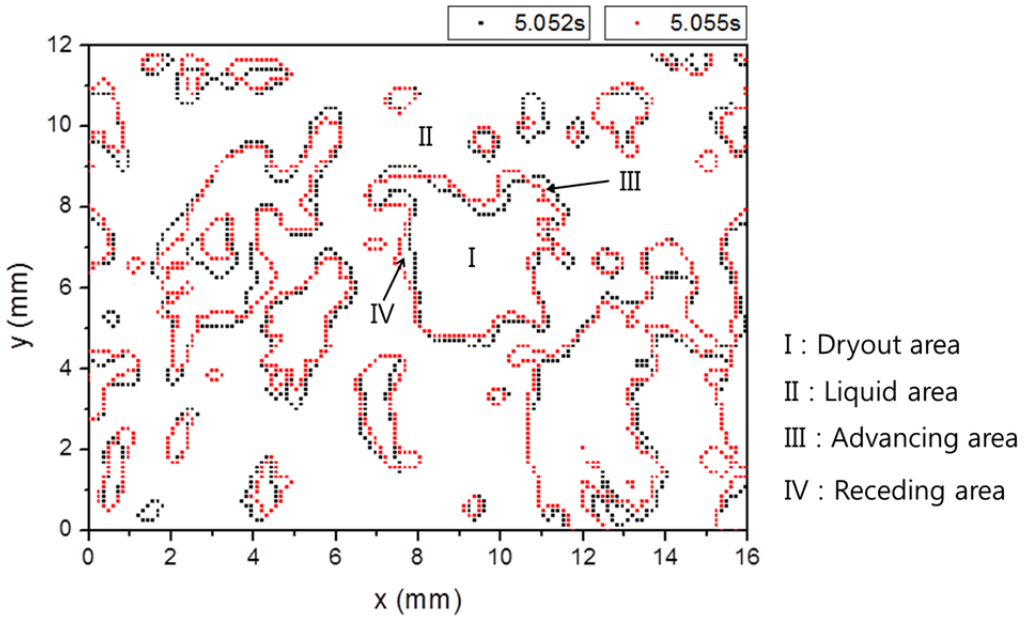

Figure 12: Heat transfer regions.

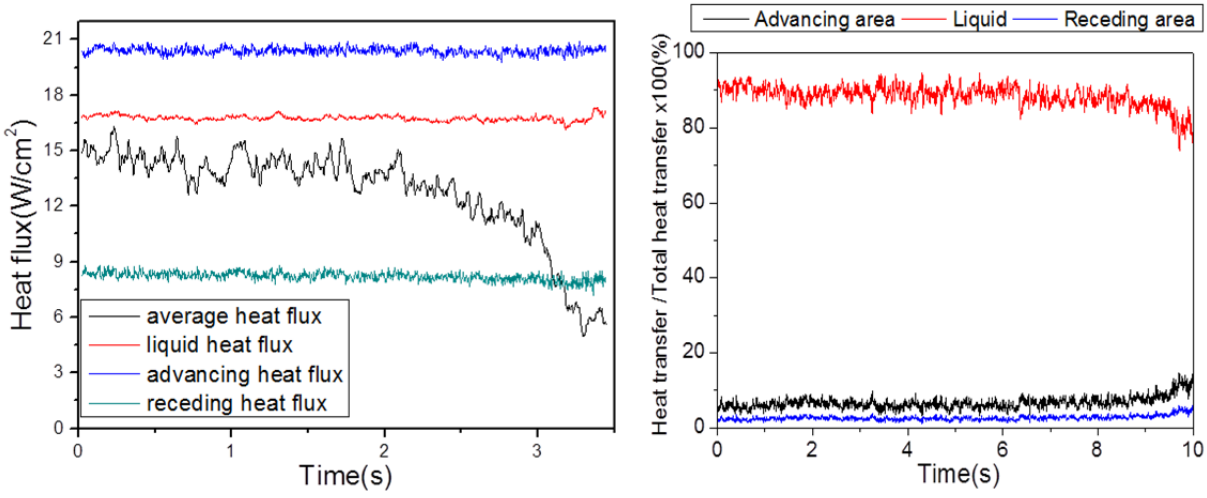

(a) Heat flux each region (b) Regional contribution for heat transfer

Figure 13: Heat flux each region and regional contribution for heat transfer at at q"=15.9W/cm^2 for ambient pressures.

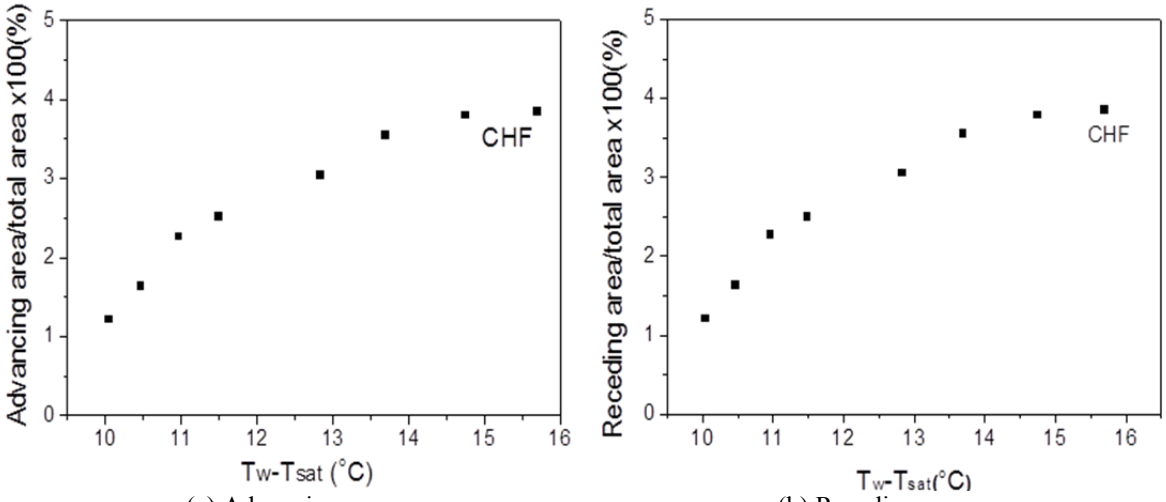

(a) Advancing area (b) Receding area

Figure 14: Advancing and receding area change with wall superheat at T_{bulk} = 56 °C for ambient pressures.

CHF Mechanism. While the heat transfer through the liquid determines the overall heat transfer, changes in the contact line heat transfer trigger the onset of CHF. When dewetting occurs in the micro region, the temperature of dryout area increases, hence the dryout area increases and CHF occurs. Based on the present observations, the following CHF mechanism has been formulated.

(A) With an increase in wall superheat, the evaporation of liquid becomes more intense, especially in the contact region. More fluid must be delivered to the contact line to feed this evaporation (Figure 14).

(B) The system promotes increased fluid flow through changes in the film profile. The adsorbed film thickness decreases, the curvature gradient increases, and the apparent contact angle increases (Figure 15).

(C) The above result in a decrease in the pressure drop that feeds fluid to micro region since the recoil pressure increases faster than the capillary pressure increases.

(D) The process of dewetting occurs the mass flux of liquid supply ($\dot{m}_{\Delta p}$) to the contact line decreases resulting in a decrease in the evaporation mass flux ($\dot{m}_q$). The lifetime of the dry spots increases as a result.

(E) The longer dry spot lifetime results in higher average temperature of dry patches (Figure 9), so the dryout area increases.

(F) The surface overheats due to less and less liquid on the surface.

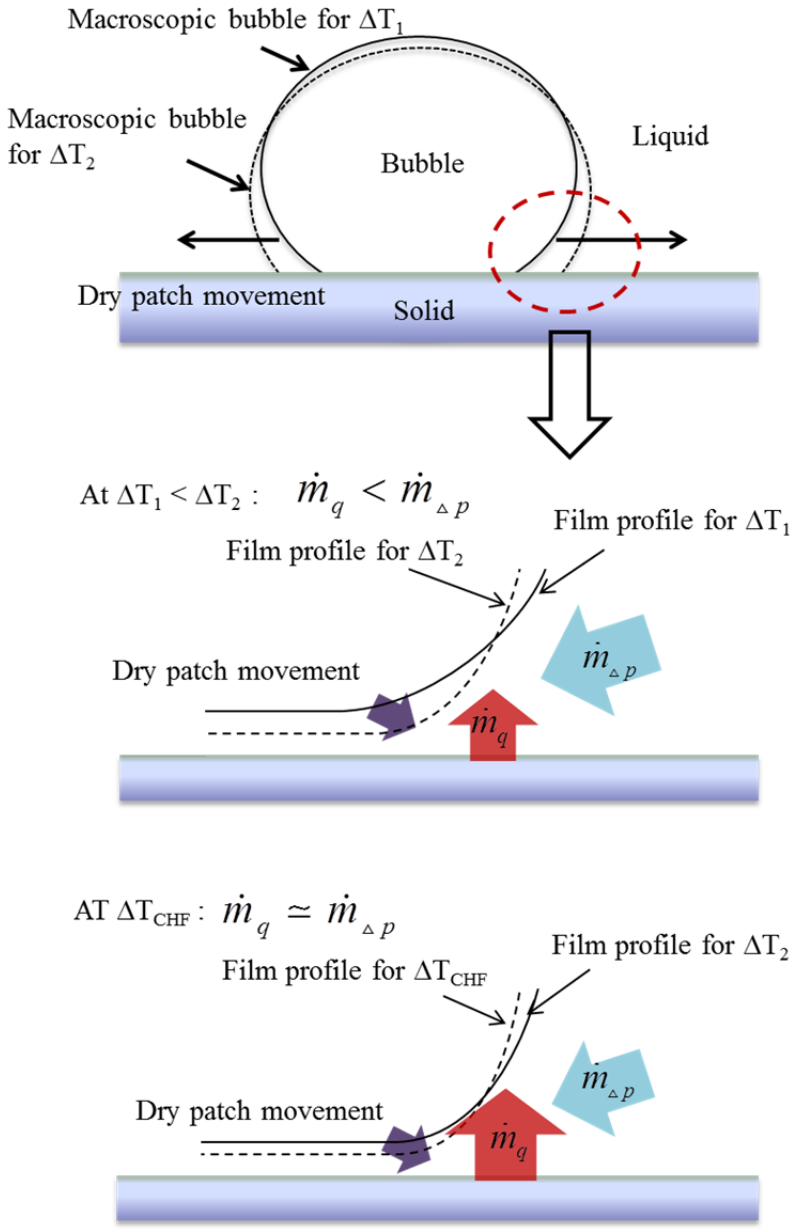

Figure 15: Illustration of the film profiles for different superheats.

CONCLUSIONS

This work provides fundamental insight into the mechanisms by which CHF is triggered. Local information on the heated surface was measured with FC-72 in pool boiling via IR camera. Using this data, space and time resolved temperature and heat flux distributions were obtained. The wetted area fraction and the contact line length density with wall superheat were obtained. Heat transfer through the liquid was found to be the dominant heat transfer mechanism to determine the overall heat transfer. It is observed that the temperature of the dry spots increases and the dryout area increases when the process of dewetting occurs at contact line and micro region. Based on the surface dewetting and experimental data, a revised CHF mechanism was proposed.

REFERENCES

Demiray, F. and Kim, J., "Microscale Heat Transfer Measurements During Pool Boiling of FC-72: Effect of Subcooling", Int. J. of Heat and Mass Transfer, Vol. 47 pp. 3257-3268, 2004.

Elbaum, M., Lipson, S.G., and Wettlaufer, J.S. (1995) "Evaporation preempts complete wetting", Europhysics Letters, Vol. 29, No. 6, pp. 457-462.

Haramura, Y. and Katto, Y.A. (1983) "A new hydrodynamic model of critical heat flux applicable widely to both pool and forced convection boiling on submerged bodies in saturated liquids", Int. J. of Heat and Mass Transfer, Vol. 26, pp. 389-399.

Horacek, B., Kiger, K., Kim, J., "Single Nozzle Spray Cooling Heat Transfer Mechanisms", Int. J. of Heat and Mass Transfer, Vol. 48, No. 8, pp. 1425-1438, 2005.

Kandilkar, S. G., 2001, "A Theoretical Model to Predict Pool Boiling CHF Incorporating Effects Contact Angle and Orientations," ASME Journal of Heat Transfer, 123, pp. 1071-1079.

Kutateladze, S. S., 1948, "On the Transition to Film Boiling Under Natural Convection," Kotloturbostroenie, No. 3, pp. 10-12.

Nishio, S., Gotoh, T. and Nagai, N. (1998), "Observation of boiling structures in high heat-flux boiling", Int. J. of Heat and Mass Transfer, Vol. 41, pp. 3191-3201.

Nishio, S. and Tanaka, H. (2004), "Visualization of boiling structures in high heat-flux pool-boiling", Int. J. of Heat and Mass Transfer, Vol. 47, pp. 4559-4568.

Raj, R., Kunkelmann, C., Stephan, P., Plawsky, J., and Kim, J., (2012) "Contact Line Behavior for a Highly Wetting Fluid Under Superheated Conditions", Int. J. of Heat and Mass Transfer, Vol. 55, pp. 2664-2675.

Taylor, G.I. and Michael, D.H. (1973) "On making holes in a sheet of fluid", J. of Fluid Mechanics, Vol. 58, pp. 625-639.

Wayner, P.C., Kao, Y.K., LaCroix, L.V. (1976) "The interline heat transfer coefficient on an evaporating wetting film", Int. J. of Heat and Mass Transfer, Vol. 19, pp. 487-492.

Zuber, N. (1959) "Hydrodynamic aspects of boiling heat transfer", AEC Report AECU-4439, Physics and Mathematics.

T.H. Kim, E. Kommer, S. Dessiatoun, and J. Kim, (2011) "Measurement of two-phase flow and heat transfer parameters using infrared thermometry", Int. J. multiphase flow, 40, 56–67. 2011.

List of Publications and Significant Collaborations that resulted from your AOARD supported project:

e) manuscripts submitted but not yet published

J. Jung, J. Kim, and S. J. Kim, "LOCAL HEAT TRANSFER MEASUREMENTS IN POOL BOILING USING INFRARED THERMOMETRY", to be presented at the 8th World conference on Experimental Heat Transfer, Fluid Mechanics, and Thermodynamics , June 16-20, 2013, Lisbon, Portugal